Supplementary Information for

Ambient blade-coated perovskite solar cells with high reverse bias stability enabled by polymeric hole transporter design

Chaoyue Zhao[1,2,†], Feifei Wang[1,†], Xiaodong Hu[1,†], Yaoyao Zhang[1],Tianxiao Liu[1], Yangyang Liu[1], Lingyuan Wang[1], Siwei Luo[1], Xiaoyu Shi[1], Xinsheng Tang[1], He Yan[2], Wei Wang[1] & Shangshang Chen[1,*]

[1]*State Key Laboratory of Coordination Chemistry, MOE Key Laboratory of High-Performance Polymer Materials & Technology, School of Chemistry and Chemical Engineering, Nanjing University, Nanjing 210023, Jiangsu, China*

[2]*Department of Chemistry and Hong Kong Branch of Chinese National Engineering Research Center for Tissue Restoration and Reconstruction, Hong Kong University of Science and Technology, Clear Water Bay, Kowloon, Hong Kong 999077, China*

†These authors contributed equally to this work.

**Corresponding author. Email: schen@nju.edu.cn (S.C.).*

Supplementary Figures

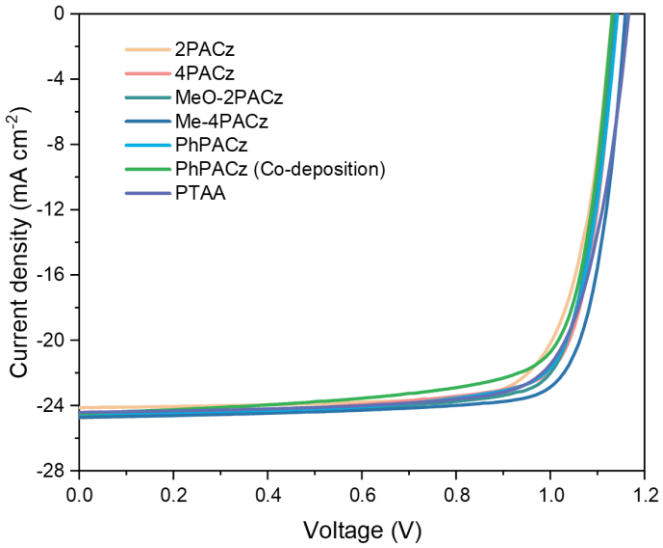

Supplementary Fig. 1. Backward *J-V* characteristic curves of the ambient blade-coated PSCs based on a variety of HTLs measured under AM 1.5G one-sun illuminance (100 mW cm^{-2}).

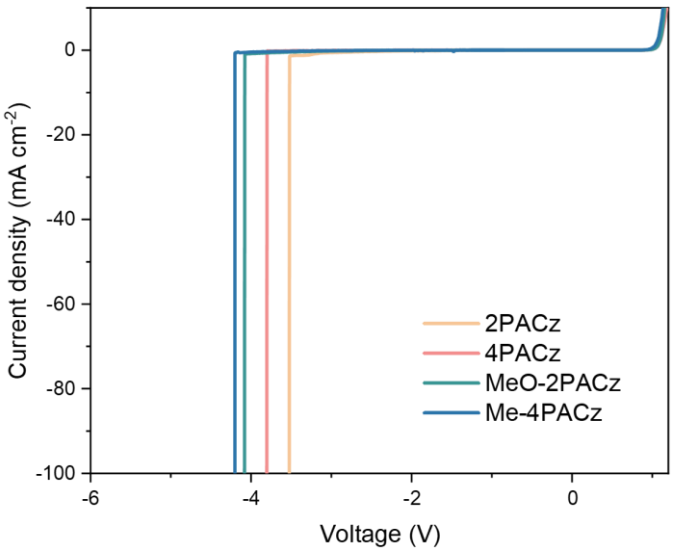

Supplementary Fig. 2. Dark *J-V* curves of the SAM-based PSCs to determine the cell V_{rb}.

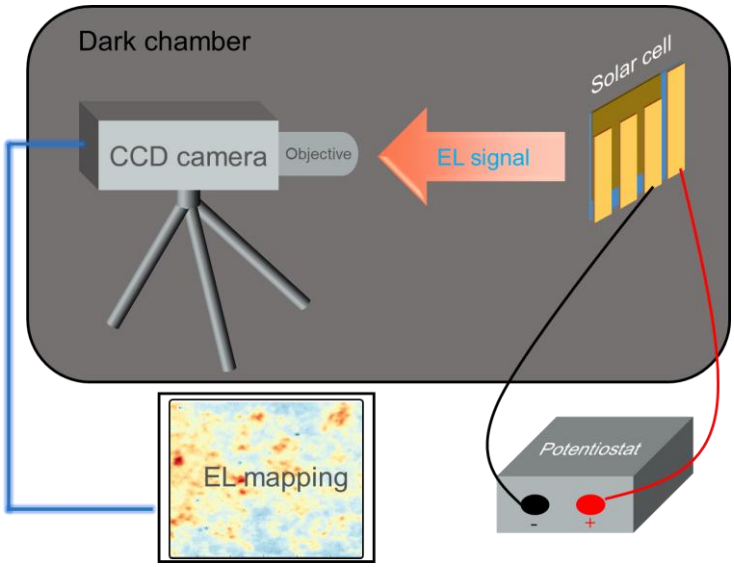

Supplementary Fig. 3. Schematic illustration of EL mapping characterization setup.

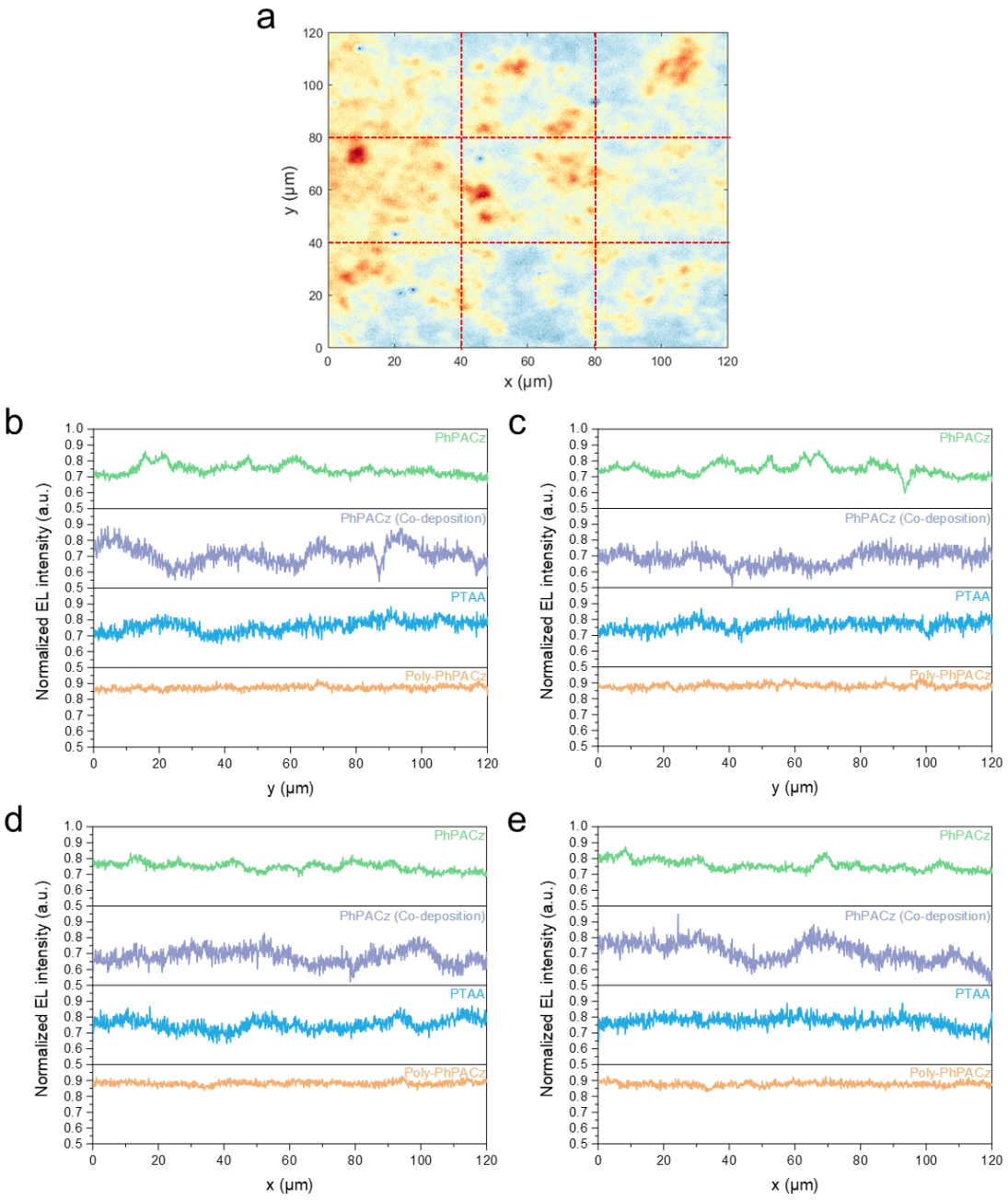

Supplementary Fig. 4. a, Schematic illustration of extracted the EL intensity profiles from 2D EL map along four lines: (**b**) x=40 μm, (**c**) x=80 μm, (**d**) y=40 μm, and (**e**) y=80 μm**.**

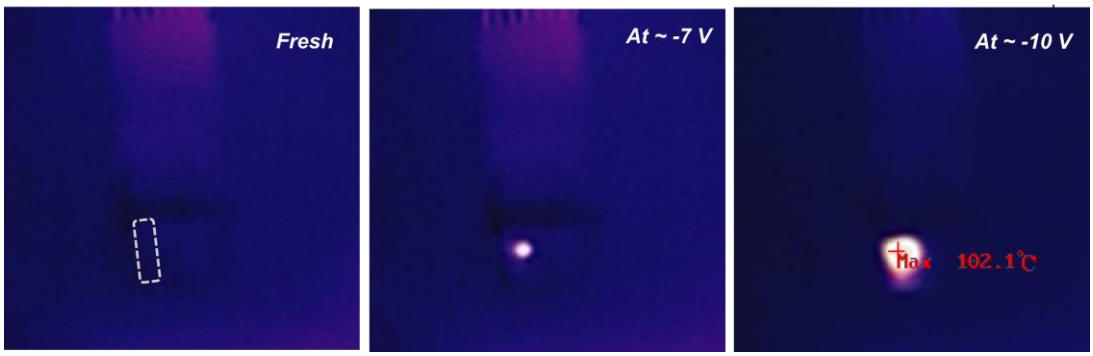

Supplementary Fig. 5. The temperature change of the Poly-PhPACz-based device under reverse bias sweeping monitored with an infrared radiometer.

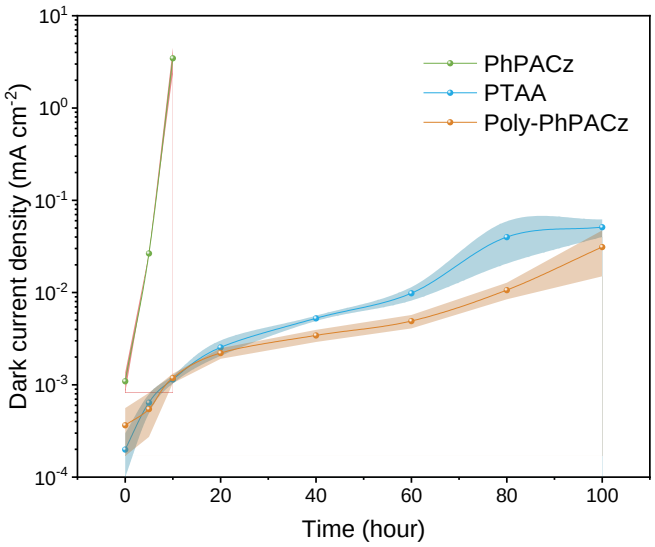

Supplementary Fig. 6. The change of dark current for different PSCs when biased at -2 V (five devices for each group). Shadow areas represent the standard deviation among devices.

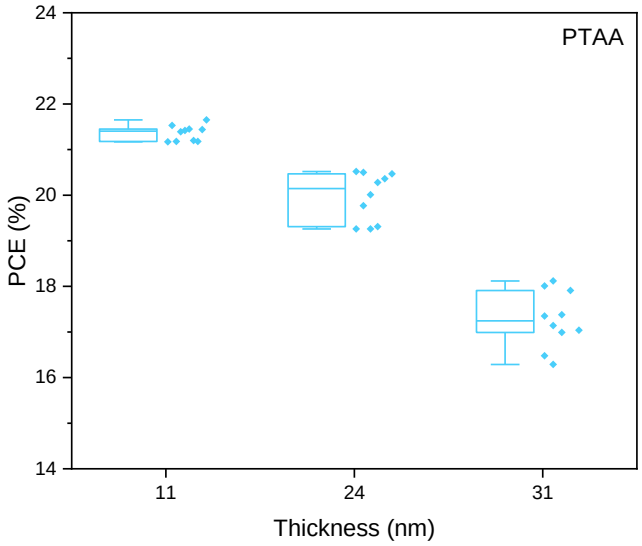

Supplementary Fig. 7. The device PCEs versus the thickness of PTAA. Box plot elements are defined as follows: center line: median; box limits: upper and lower quartiles; whiskers: 1.5× interquartile range.

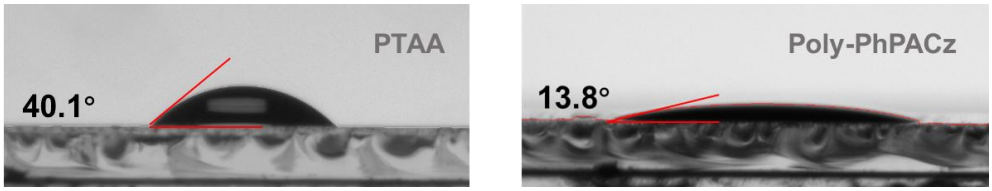

Supplementary Fig. 8. Contact angles of the perovskite ink on the ITO substrates coated with PTAA and Poly-PhPACz.

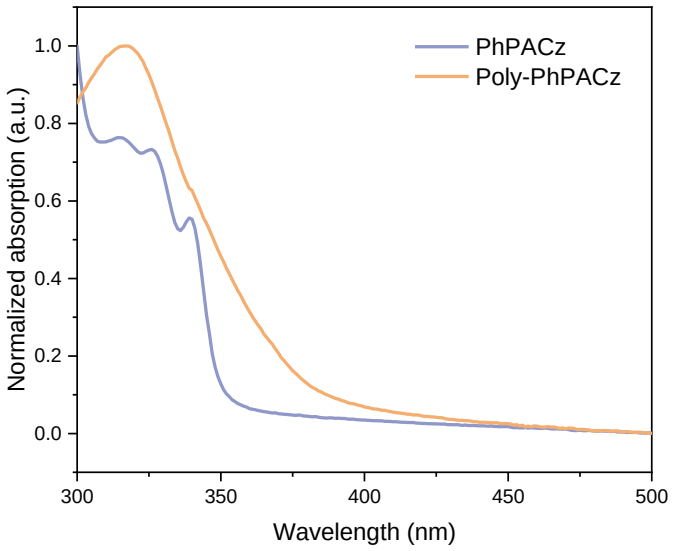

Supplementary Fig. 9. Normalized UV-vis absorption spectra of PhPACz and Poly-PhPACz films.

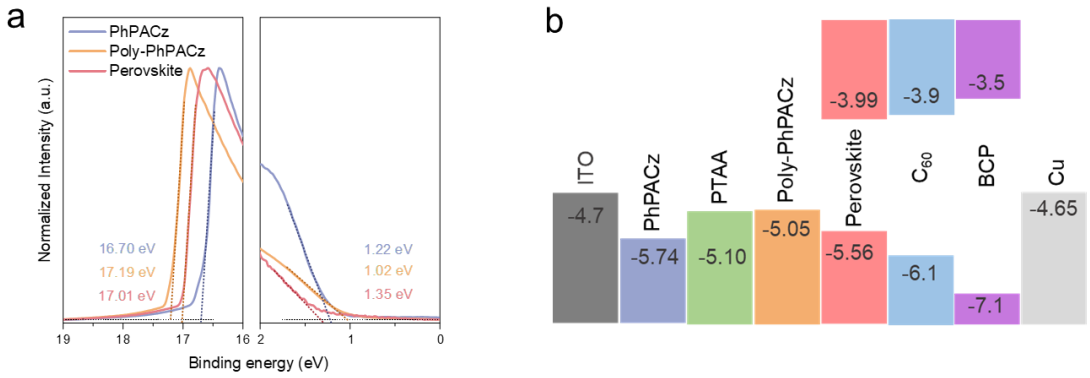

Supplementary Fig. 10. a, UPS spectra of PhPACz film, Poly-PhPACz film and perovskite film on ITO glass substrates. **b**, Summary for energy levels of each layer involved in the PSCs.

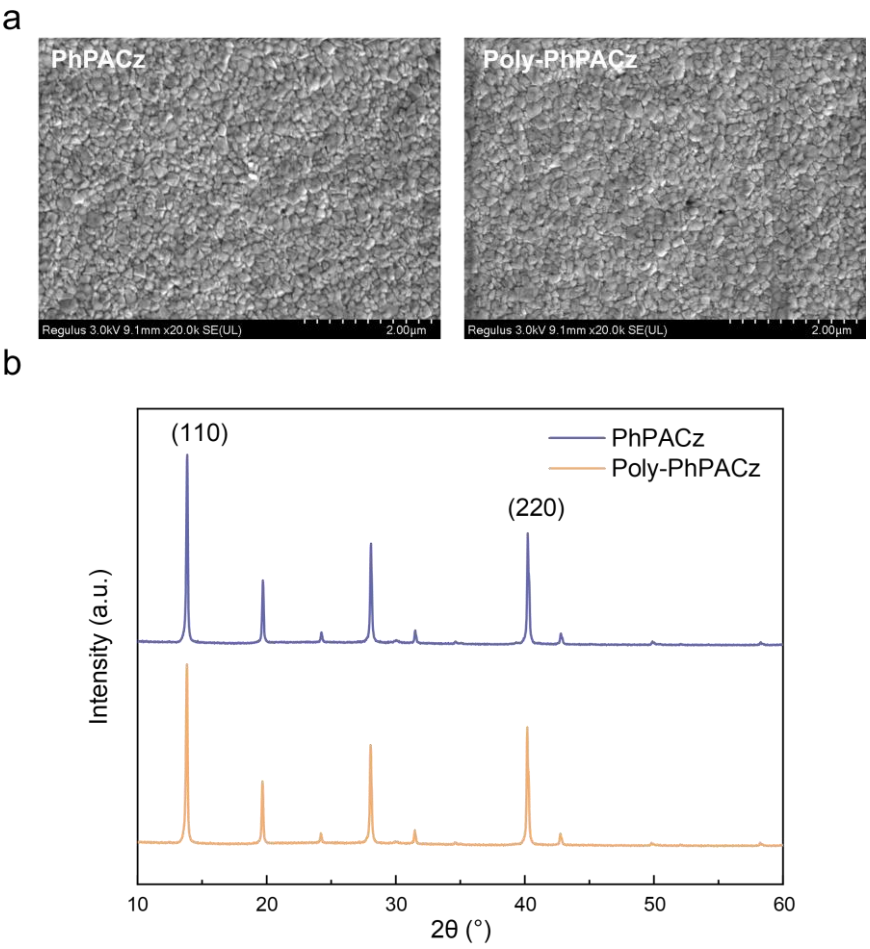

Supplementary Fig. 11. Top-view SEM images (**a**) and XRD patterns (**b**) of the perovskite films deposited on PhPACz and Poly-PhPACz.

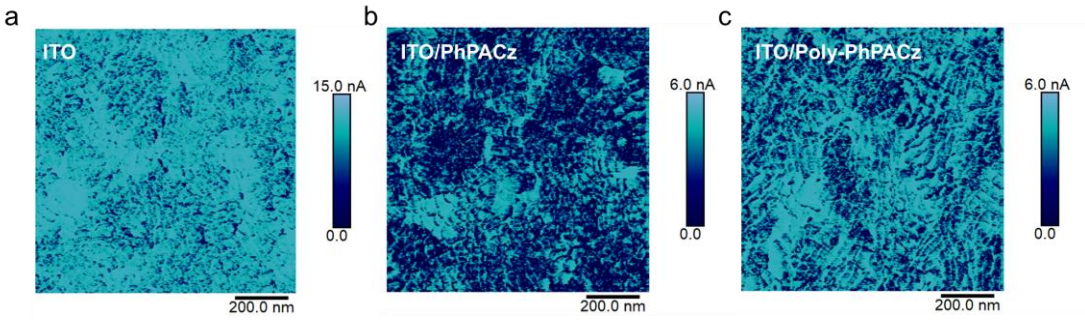

Supplementary Fig. 12. c-AFM current images of (**a**) bare ITO and ITO substrates coated with (**b**) PhPACz and (**c**) Poly-PhPACz.

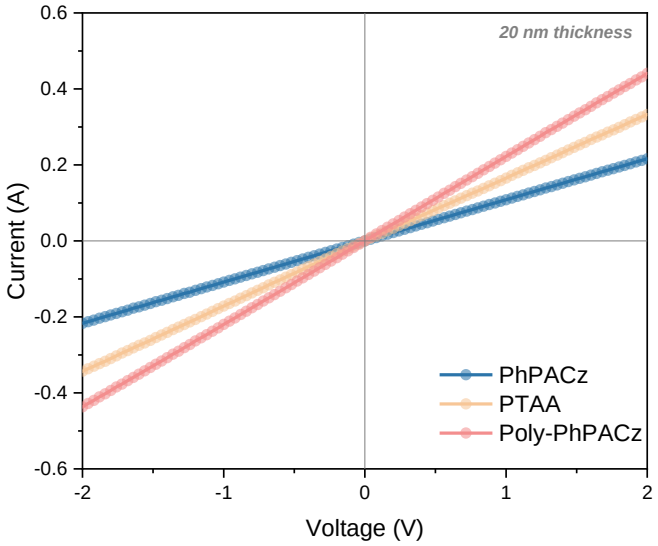

Supplementary Fig. 13. *I-V* curves of the glass/ITO/HTL (20 nm)/Ag devices.

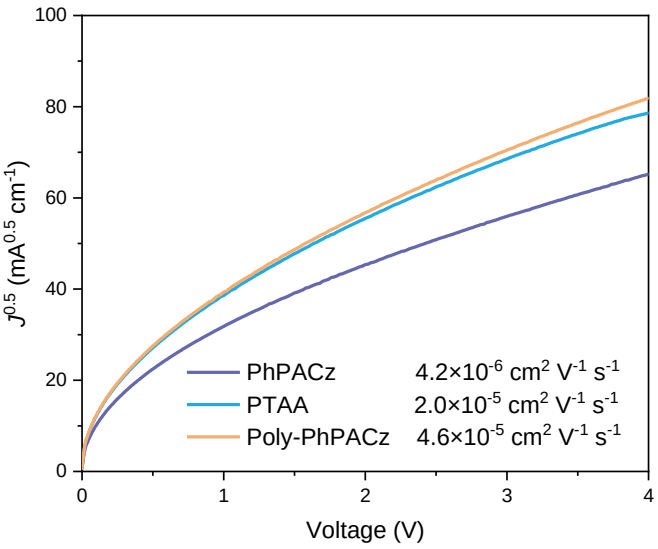

Supplementary Fig. 14. $J^{1/2}$ versus V characteristic curves of the hole-only devices based on three HTLs.

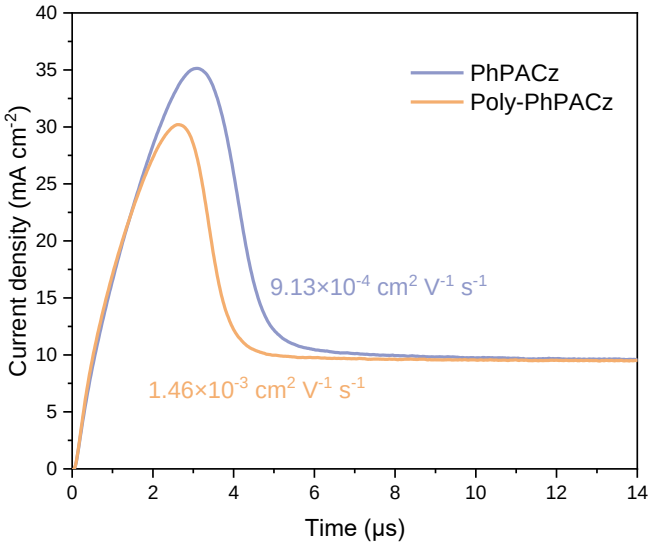

Supplementary Fig. 15. Photo-CELIV curves of the PSCs based on PhPACz and Poly-PhPACz.

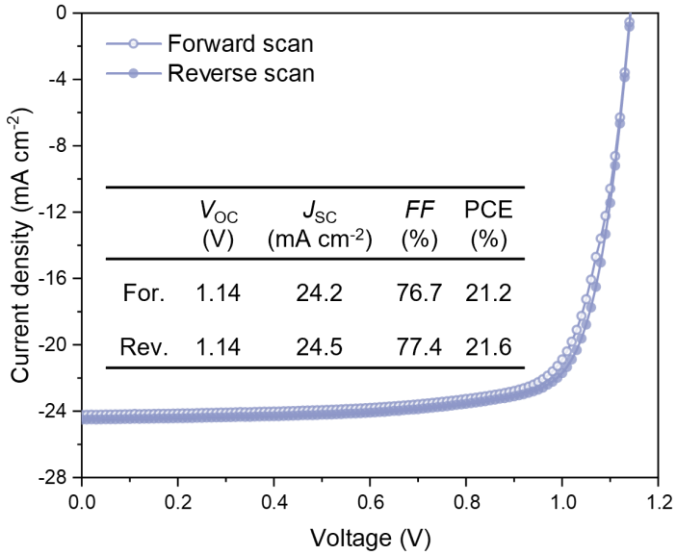

Supplementary Fig. 16. Reverse and forward *J-V* characteristic curves of the PSCs based on PhPACz. Inset shows the device parameters derived from the curves.

Chengdu Institute of Product Quality Inspection Co., Ltd.
National Photovoltaic Product Quality Inspection &Testing Center
TEST REPORT

Test Report No. AGXB125W00136 Page 3 of 3

Test Results（Reverse scanning）:

No.	Test item(s)	Unit	Results
2	Current-voltage characteristics measurement	---	---
2.1	Open-circuit voltage, V_{OC}	V	1.171
2.2	Short-circuit current, I_{SC}	mA	1.160
2.3	Maximum-power, P_{max}	mW	1.122
2.4	Maximum-power voltage, $V_{p\text{-}max}$	V	1.020
2.5	Maximum-power current, $I_{p\text{-}max}$	mA	1.100
2.6	Fill factor, FF	%	82.60
2.7	Conversion efficiency, η	%	25.85

Current-voltage characteristics under STC

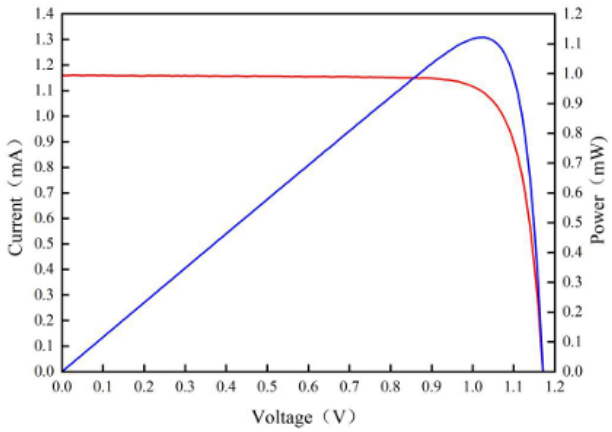

Remark: Sample was tested under the irradiation with a steady-state class calibrated AAA solar simulator (AM1.5-G 1000.0 W/m² basted on mono-Si reference cell) at 25±1 °C. Designated area defined by thin metal aperture mask.
The measuring uncertainty : U_{rel}(Pmax)=2.85%(k=2); U_{rel}(Isc)=2.69%(k=2); U_{rel}(Voc)=1.57%(k=2).

————Blank————

Supplementary Fig. 17-1. Certification report of the champion PSC based on Poly-PhPACz.

Chengdu Institute of Product Quality Inspection Co., Ltd.
National Photovoltaic Product Quality Inspection &Testing Center
TEST REPORT

Test Report No.AGXB125W00136 Page 2 of 3

Test Results（Forward scanning）:

No.	Test item(s)	Unit	Results
1	Current-voltage characteristics measurement	---	---
1.1	Open-circuit voltage, V_{OC}	V	1.161
1.2	Short-circuit current, I_{SC}	mA	1.152
1.3	Maximum-power, P_{max}	mW	1.098
1.4	Maximum-power voltage, $V_{p\text{-}max}$	V	1.030
1.5	Maximum-power current, $I_{p\text{-}max}$	mA	1.066
1.6	Fill factor, FF	%	82.09
1.7	Conversion efficiency, η	%	25.30

Current-voltage characteristics under STC

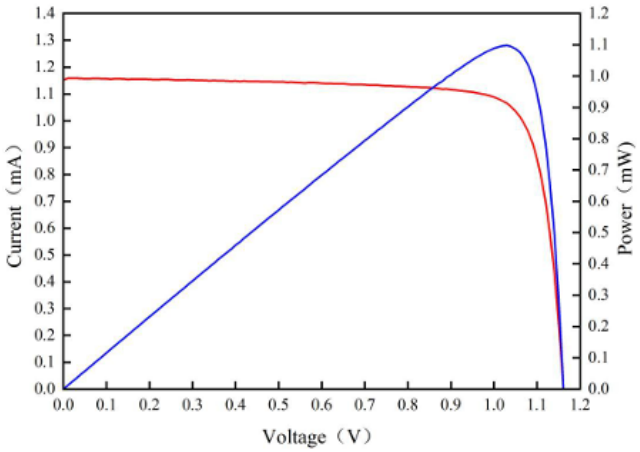

Remark: Sample was tested under the irradiation with a steady-state class calibrated AAA solar simulator (AM1.5-G 1000.0 W/m² basted on mono-Si reference cell) at 25±1 °C. Designated area defined by thin metal aperture mask.
The measuring uncertainty : U_{rel}(Pmax)=2.85%(k=2); U_{rel}(Isc)=2.69%(k=2); U_{rel}(Voc)=1.57%(k=2).

Supplementary Fig. 17-2. Certification report of the champion PSC based on Poly-PhPACz..

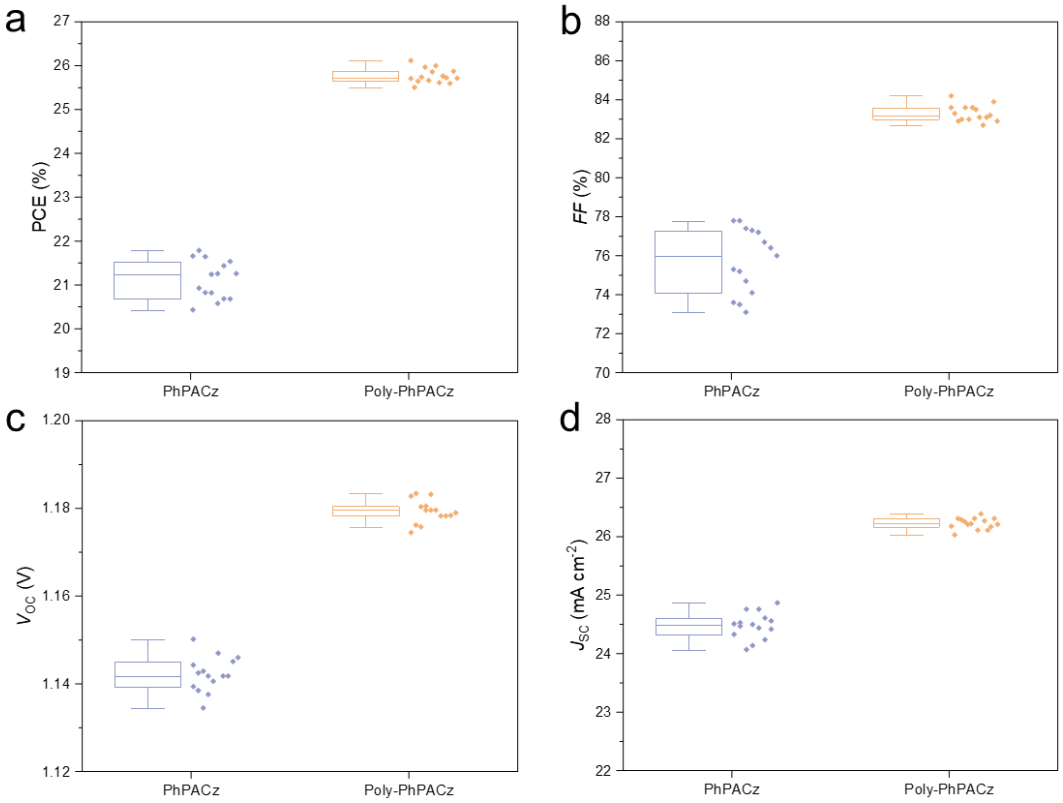

Supplementary Fig. 18. Statistical results of (**a**) PCE, (**b**) *FF*, (**c**) V_{OC}, and (**d**) J_{SC} for the PSCs based on PhPACz and Poly-PhPACz. Box plot elements in are defined as follows: center line: median; box limits: upper and lower quartiles; whiskers: 1.5× interquartile range.

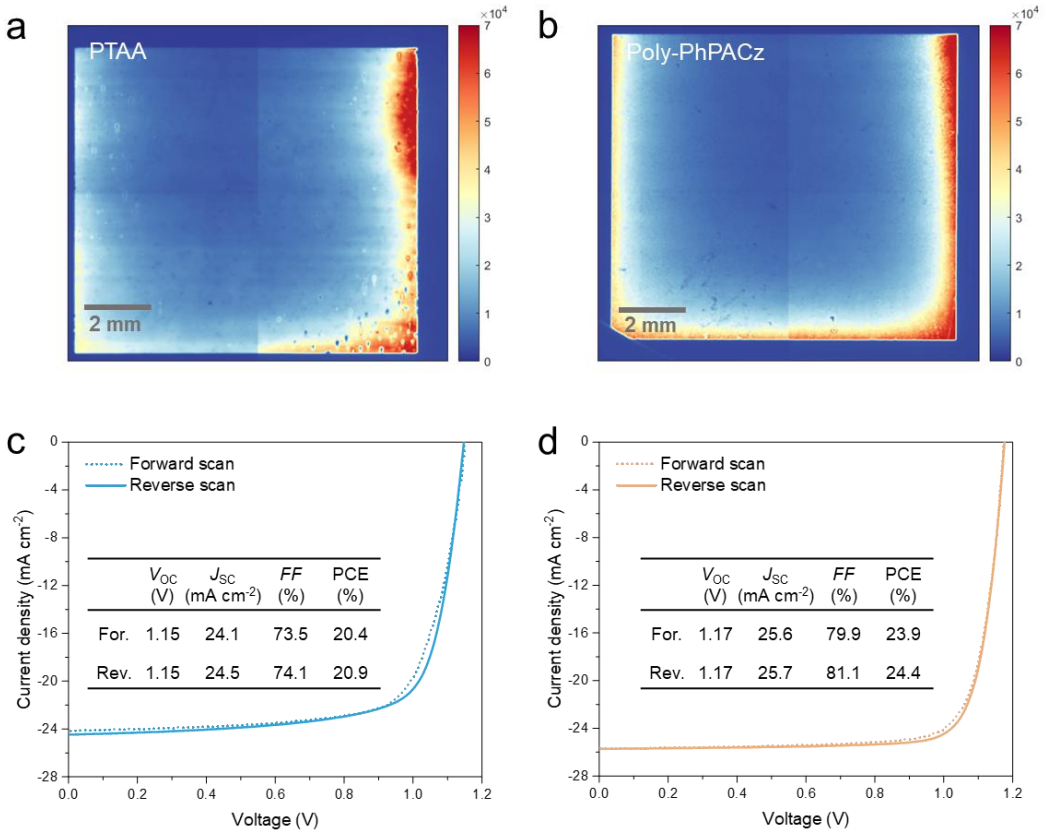

Supplementary Fig. 19. EL mapping (**a,b**) and *J-V* characteristic curves (**c,d**) of the1-cm^2 PSCs based on PTAA and Poly-PhPACz. Insets in (**c,d**) show the detailed photovoltaic parameters.

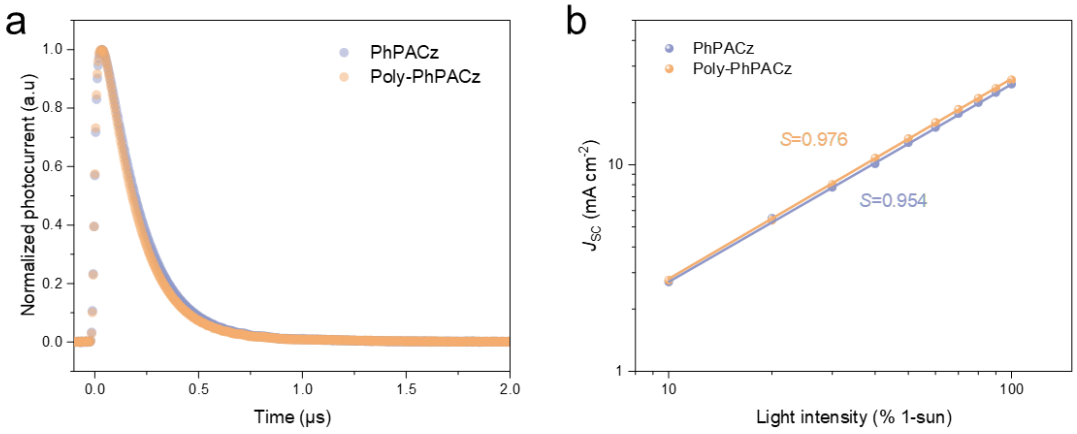

Supplementary Fig. 20. (**a**) TPC spectra and (**b**) J_{SC} versus light intensity curves of the PSCs based on PhPACz and Poly-PhPACz.

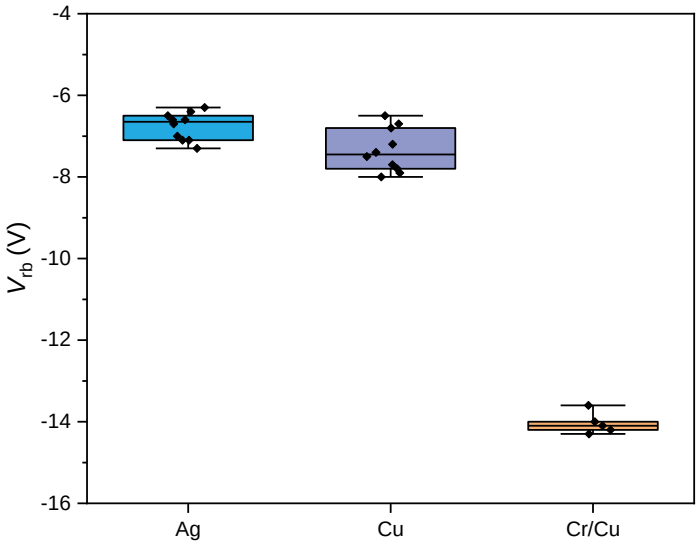

Supplementary Fig. 21. V_{rb} distribution of the PSCs based on Ag, Cu, and Cr/Cu electrodes. Box plot elements in are defined as follows: center line: median; box limits: upper and lower quartiles; whiskers: 1.5× interquartile range.

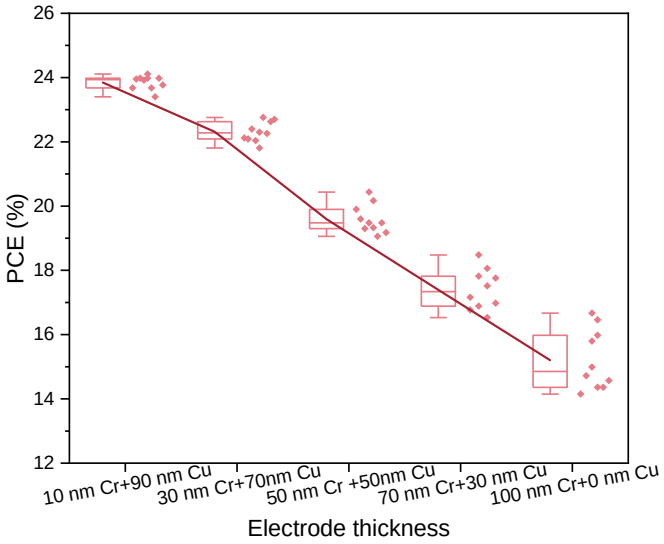

Supplementary Fig. 22. Device PCE versus Cr thickness of the double-layer electrode. Box plot elements in are defined as follows: center line: median; box limits: upper and lower quartiles; whiskers: 1.5× interquartile range.

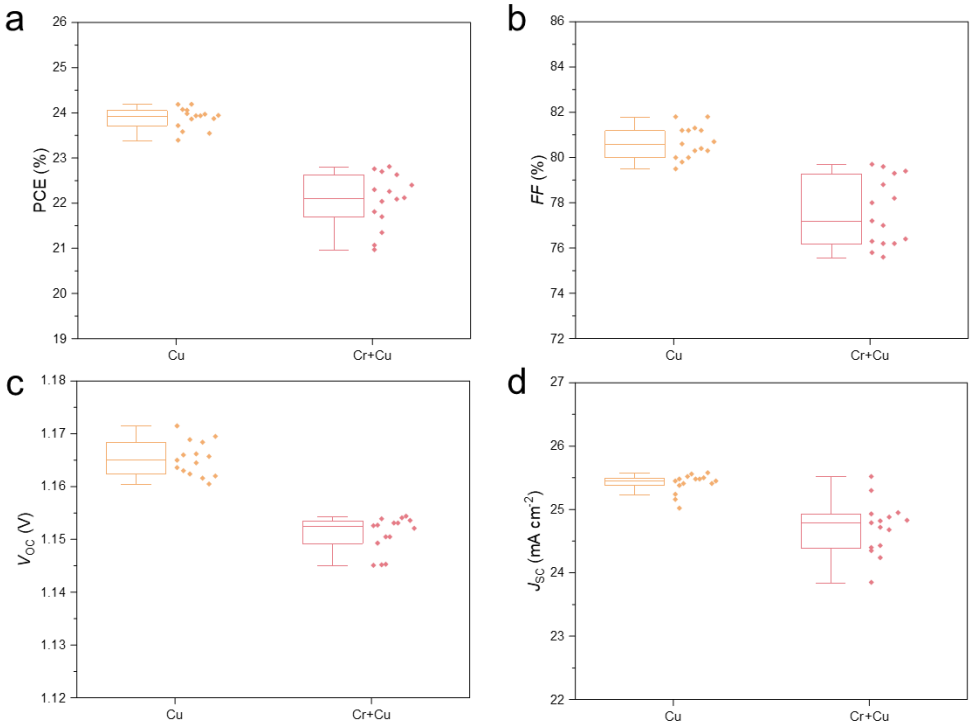

Supplementary Fig. 23. Statistical results of (**a**) PCE, (**b**) *FF*, (**c**) V_{OC}, and (**d**) J_{SC} for the devices based on Cu and Cr/Cu electrodes. Box plot elements are defined as follows: center line: median; box limits: upper and lower quartiles; whiskers: 1.5× interquartile range.

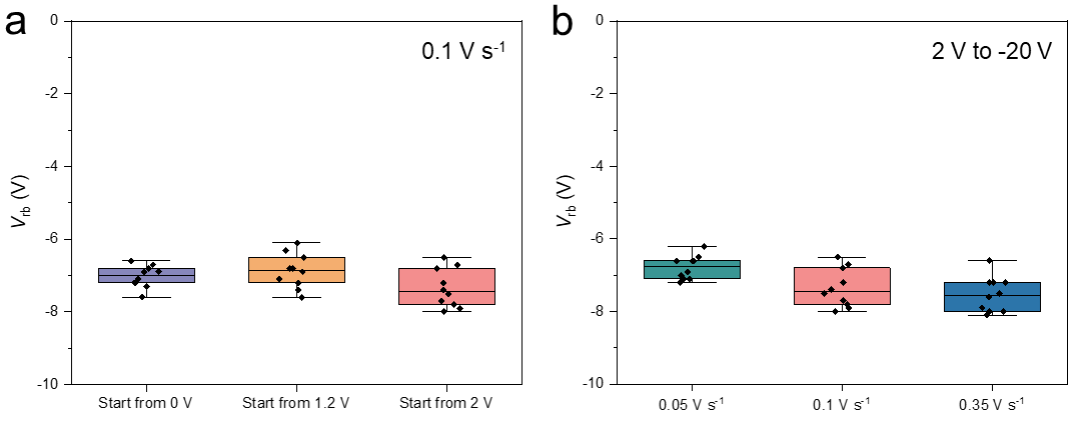

Supplementary Fig. 24. V_{rb} distribution of the Poly-PhPACz-based PSCs swept from different start voltage (**a**) and different scan rate (**b**). Box plot elements in are defined as follows: center line: median; box limits: upper and lower quartiles; whiskers: 1.5× interquartile range.

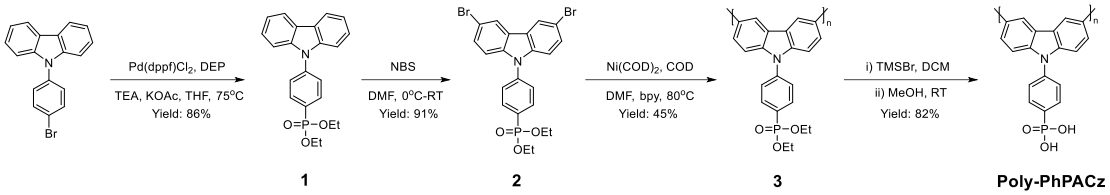

Supplementary Fig. 25. Synthesis route of Poly-PhPACz.

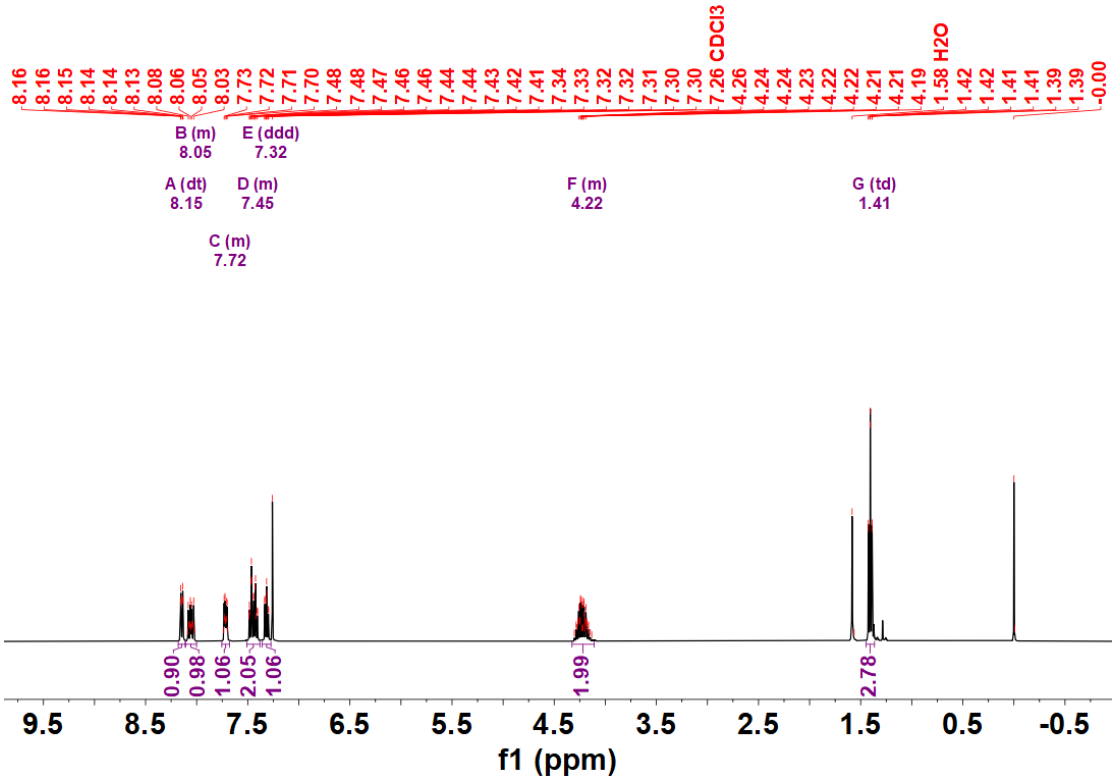

Supplementary Fig. 26. ^{1}H NMR spectrum of compound 1.

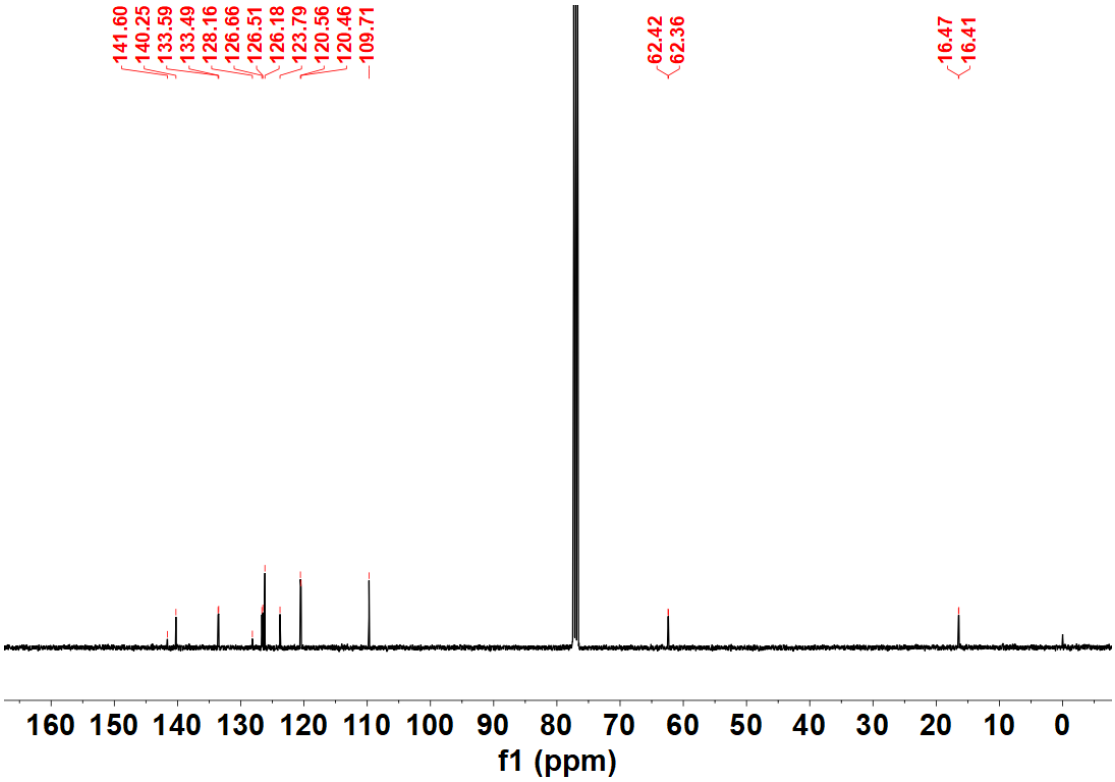

Supplementary Fig. 27. ^{13}C NMR spectrum of compound 1.

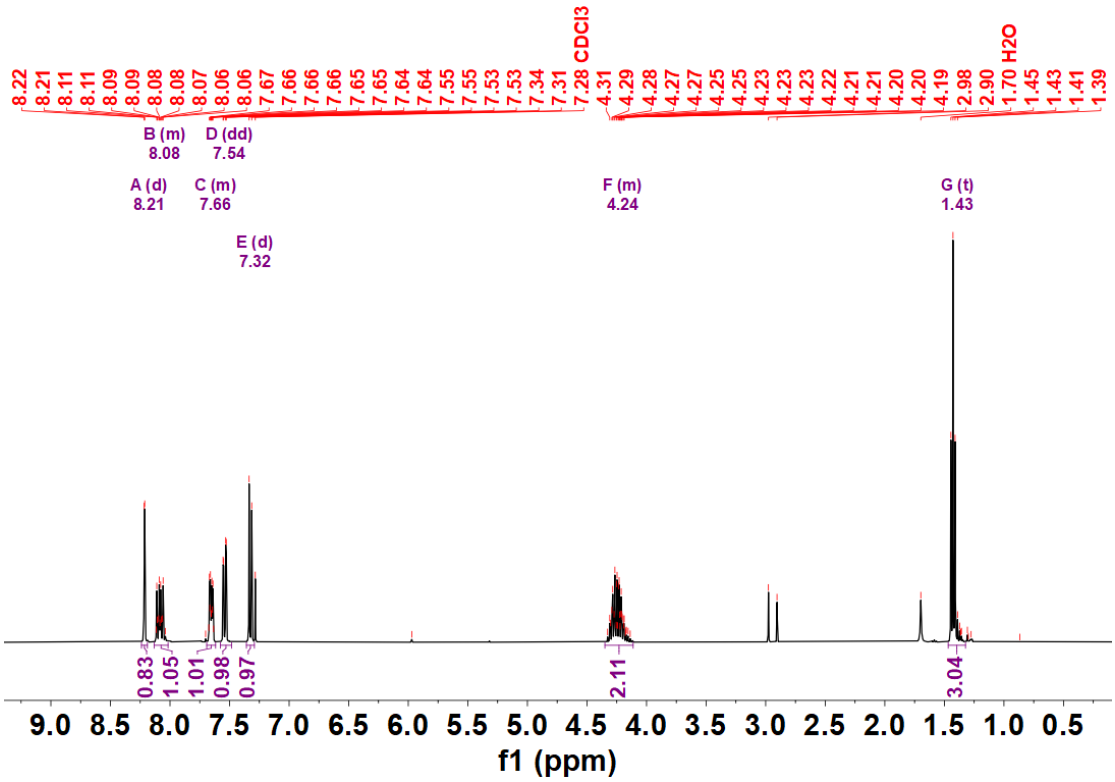

Supplementary Fig. 28. ^{1}H NMR spectrum of compound 2.

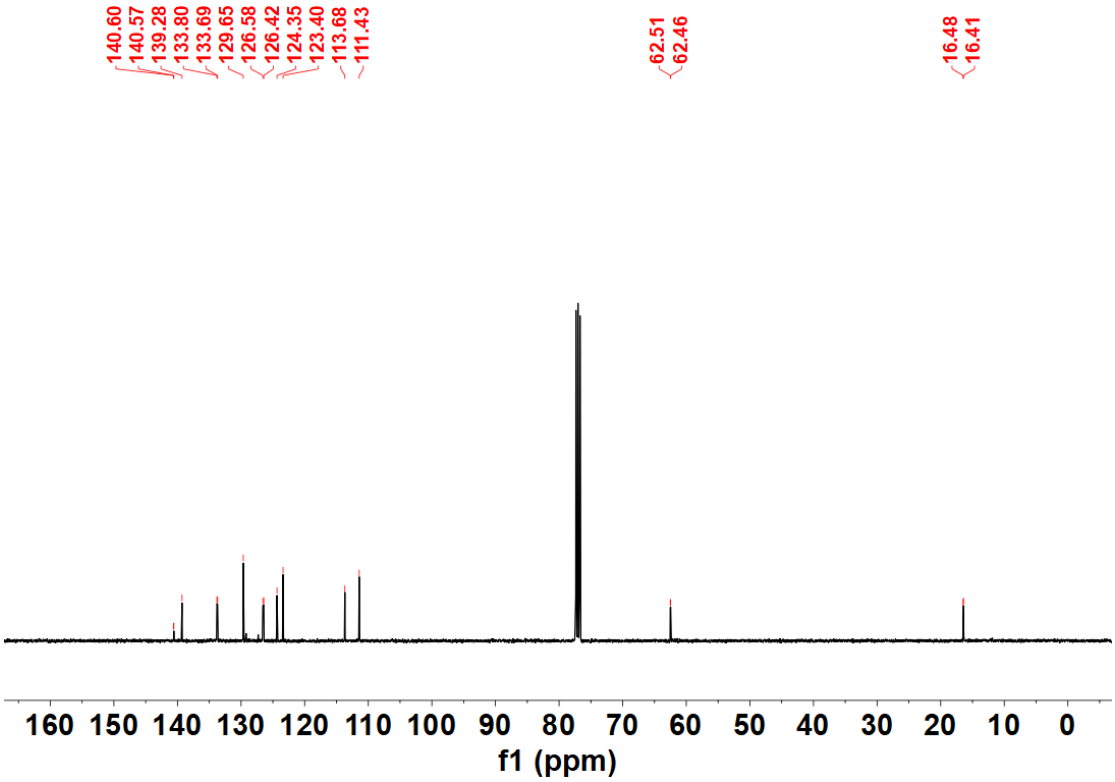

Supplementary Fig. 29. ^{13}C NMR spectrum of compound 2.

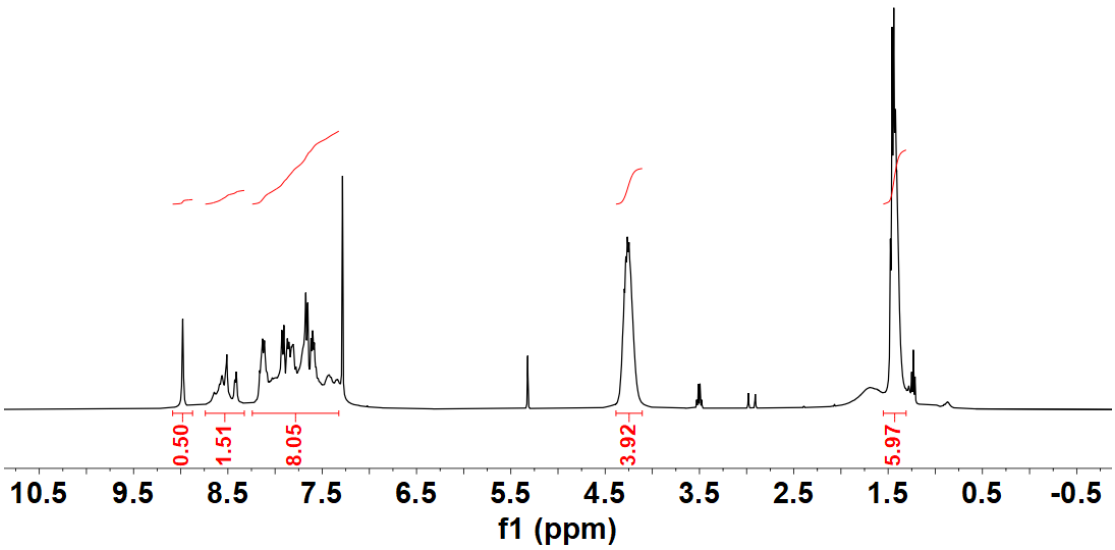

Supplementary Fig. 30. ^{1}H NMR spectrum of compound 3.

Supplementary Note

To investigate the influence of the bias conditions (scan range and rate) on the V_{rb} of devices, three different scan ranges were selected: 0 to −20 V, 1.2 to −20 V, and 2 to −20 V, along with three scan rates including 0.05 V s^{-1}, 0.10 V s^{-1}, and 0.35 V s^{-1}. The corresponding V_{rb} values are summarized in Supplementary Fig. 24. With respect to the bias scan range, a higher starting positive voltage had almost no detrimental effect on V_{rb}, which is attributed to the relatively short duration of applied forward bias in this study. Regarding the scan rate, we found that at a high rate of 0.35 V s^{-1}, the V_{rb} values were comparable to those measured at 0.1 V s^{-1}. This result is consistent with the report by Ginger *et al.* (*Nat. Energy* 2024, 9, 1275), which indicated that within a reasonable range, the scan rate has limited impact on V_{rb}. As the focus of current work is to evaluate and compare the reverse-bias stability of different HTLs, we employed a bias condition adopted from a well-established protocol reported by Ginger *et al.*, and the scan rate is 0.10 V s^{-1} from 2 V to −20 V under dark to ensure fair and direct comparison of their robustness under reverse bias.

Supplementary Method

The synthesis route of Poly-PhPACz is shown in Supplementary Fig. 25. Below are the synthesis details.

Diethyl(4-(9H-carbazol-9-yl)phenyl)phosphonate (1): 9-(4-bromophenyl)-9H-carbazole (1.0 equiv, 1.4 g, 4.3 mmol), Pd(dppf)Cl_2 (0.05 equiv, 165 mg, 0.22 mmol), KOAc (0.3 equiv, 132 mg, 1.3 mmol) were placed in a 50 ml Schlenk tube equipped with a stirring bar. The tube was then evacuated and back-filled with argon for three times. To these solids, anhydrous THF (20 ml), TEA (2.2 equiv, 1.4 ml, 9.5 mmol), diethyl phosphite (DEP, 2.2 equiv, 1.3 ml, 9.5 mmol) were added via a gastight syringe under argon atmosphere. The reaction mixture was stirred at 75°C for 12 h. The mixture was quenched with brine and extracted with ethyl acetate (3 × 10 ml). The organic layers were combined and concentrated under vacuum. The residue was purified by silica gel column chromatography to obtain a white solid (1.4 g, yield: 86%).

^{1}H NMR (400 MHz, Chloroform-*d*) δ 8.15 (dt, *J* = 7.8, 1.1 Hz, 1H), 8.11 – 8.00 (m, 1H), 7.75 – 7.68 (m, 1H), 7.51 – 7.38 (m, 2H), 7.32 (ddd, *J* = 8.0, 6.9, 1.2 Hz, 1H), 4.33 – 4.11 (m, 2H), 1.41 (td, *J* = 7.0, 0.5 Hz, 3H).

^{13}C NMR (101 MHz, $CDCl_3$) δ 141.60, 140.25, 133.59, 133.49, 128.16, 126.66, 126.51, 126.18, 123.79, 120.56, 120.46, 109.71, 62.42, 62.36, 16.47, 16.41.

HRMS (ESI+) m/z: $[M+H]^+$ calcd for $C_{22}H_{22}NO_3P^+$ 380.1416; found 380.1395.

Diethyl(4-(3,6-dibromo-9H-carbazol-9-yl)phenyl)phosphonate (2): To a stirred solution of compound 1 (1 equiv, 500 mg, 1.3 mmol) in DMF (5 ml), NBS (2 equiv, 469 mg, 2.6 mmol) was added slowly at 0°C. After the addition, the mixture was stirred for 12 h at room temperature. Then, the solution was poured into 250 mL cold water and extracted with ethyl acetate (3 × 10 ml). The organic layers were combined and concentrated under vacuum. The residue was purified by silica gel column chromatography to obtain a white solid (644 mg, yield: 91%).

^{1}H NMR (400 MHz, Chloroform-*d*) δ 8.21 (d, *J* = 1.9 Hz, 1H), 8.13 – 8.02 (m, 1H), 7.69 – 7.62 (m, 1H), 7.54 (dd, *J* = 8.8, 2.0 Hz, 1H), 7.32 (d, *J* = 8.8 Hz, 1H), 4.35 – 4.11 (m, 2H), 1.43 (t, *J* = 7.1 Hz, 3H).

^{13}C NMR (101 MHz, $CDCl_3$) δ 140.60, 140.57, 139.28, 133.80, 133.69, 129.65, 126.58, 126.42, 124.35, 123.40, 113.68, 111.43, 62.51, 62.46, 16.48, 16.41.

HRMS (ESI+) m/z: $[M+H]^+$ calcd for $C_{22}H_{21}Br_2NO_3P^+$ 537.9605; found 537.9583.

Poly-diethyl (4-(3,6-dibromo-9H-carbazol-9-yl)phenyl)phosphonate (3): $Ni(COD)_2$ (1.2 equiv, 220 mg, 0.80 mmol), 2,2'-bipyridine (1.2 equiv, 152 mg, 0.80 mmol) and cyclooctadiene (1.2 equiv, 0.102 ml, 0.80 mmol) were added into 25 ml DMF under nitrogen and the mixture was stirred at 80°C for 30 minutes. Next, compound 2 (1 equiv, 360 mg, 0.67 mmol) in 5 ml DMF was added dropwise, then the reaction mixture was stirred at 80°C for 12 hrs. After the reaction completed, the mixture was diluted with 1 M HCl (90 ml) and extracted with DCM (30 ml × 3). The organic layers were combined and washed with 0.01 M EDTA (30 ml × 3) and water (30 ml × 3). The organic phase was dried over anhydrous $MgSO_4$, then filtered and concentrated under reduced pressure to obtain a grey solid (0.122 g, yield: 45%).

^{1}H NMR (400 MHz, Chloroform-*d*) δ 8.51 (td, *J* = 40.1, 36.8, 12.8 Hz, 2H), 8.24 – 7.32 (m, 8H), 4.28 (ddq, *J* = 23.9, 16.8, 9.2, 8.0 Hz, 4H), 1.43 (dd, *J* = 14.1, 6.9 Hz, 6H).

GPC analysis: M_n = 1809 g mol^{-1}, M_w = 2876 g mol^{-1}, PDI = 1.6.

Poly-PhPACz: To a solution of compound 3 (1 equiv, 64 mg) in DCM was added TMSBr (2.5 equiv, 65 mg). The reaction mixture was stirred at room temperature for 12 hrs. After the reaction was completed, methanol was added to the mixture and stirred for 12 hrs. The solution was concentrated and dropped into ether 3 times to obtain a brown solid (54 mg, yield: 82%). It should be noted that phosphonate groups may not

fully convert to phosphonic acid during the hydrolysis process. The NMR spectra related to the synthesis of Poly-PhPACz can be found in Supplementary Figs. 26 to 30.

Supplementary Tables

Supplementary Table 1. Photovoltaic parameters of the PSCs based on a variety of HTLs.

HTL	V_{OC} (V)	J_{SC} (mA cm^{-2})	*FF* (%)	PCE (%)
2PACz	1.13	24.1	77.0	21.0
4PACz	1.14	24.8	77.7	22.0
MeO-2PACz	1.14	24.7	78.8	22.2
Me-4PACz	1.16	24.7	79.8	22.9
PhPACz	1.14	24.5	77.4	21.6
PhPACz (Co-deposition)	1.13	24.5	75.3	20.8
PTAA	1.17	24.4	76.0	21.7

Supplementary Table 2. Summary of the fitting parameters for the TRPL spectra using the bi-exponential decay function $y = y_0+A_1exp(-x/t_1)+A_2exp(-x/t_2)$, $t_{ave} = (A_1t_1^2+A_2t_2^2)/(A_1t_1+A_2t_2)$.

Sample	A_1	t_1 (ns)	A_2	t_2 (ns)	t_{avg} (ns)
PhPACz/Perovskite	0.379	41.2	0.187	2130.8	2051.9
Poly-PhPACz/Perovskite	0.313	51.3	0.287	2708.8	2655.0

Supplementary Table 3. Photovoltaic parameters of the PSCs based on PhPACz and Poly-PhPACz. The data in parentheses are statistical results.

HTL	V_{OC} (V)	J_{SC} (mA cm^{-2})	*FF* (%)	PCE (%)
PhPACz	1.14	24.5	77.4	21.6
	(1.14±0.004)	(24.4±0.3)	(75.7±1.6)	(21.1±0.4)
Poly-PhPACz	1.18	26.2	84.3	26.1
	(1.18±0.003)	(26.2±0.2)	(83.3±0.4)	(25.8±0.2)

Supplementary Table 4. Photovoltaic parameters of the Poly-PhPACz PSCs based on Cu and Cr/Cu electrodes. The data in parentheses are statistical results.

Electrode	V_{OC} (V)	J_{SC} (mA cm^{-2})	*FF* (%)	PCE (%)
Cu	1.16	25.5	81.8	24.2
	(1.17±0.003)	(25.4±0.1)	(80.7±0.7)	(23.9±0.2)
Cr/Cu (30 nm + 70 nm)	1.15	24.8	79.7	22.7
	(1.15±0.003)	(24.7±0.4)	(77.6±1.4)	(22.1±0.6)

Supplementary Table 5. The evolution of device photovoltaic parameters after being biased at −2 V bias for different duration.

Electrode	Aging duration (h)	V_{OC} (V)	J_{SC} (mA cm^{-2})	*FF* (%)	PCE (%)
Cu	0	1.17	25.6	79.0	23.7
	5	1.16	25.4	77.7	22.9
	10	1.16	25.6	75.5	22.4
	20	1.16	25.5	74.3	22.0
	40	1.16	25.5	72.1	21.3
	60	1.16	25.5	71.4	21.1
	80	1.16	25.4	68.5	20.2
	100	1.15	25.3	64.8	18.9
Cr/Cu (30 nm+ 70 nm)	0	1.15	24.8	79.9	22.8
	5	1.15	24.7	79.4	22.6
	10	1.16	24.7	79.1	22.7
	20	1.15	24.8	78.6	22.4
	40	1.15	24.7	78.7	22.4
	60	1.15	24.7	78.1	22.2
	80	1.15	24.6	77.4	21.9
	100	1.15	24.6	77.1	21.8
	120	1.14	24.3	76.4	21.2
	140	1.14	24.4	74.3	20.7
	160	1.14	24.4	73.5	20.4
	180	1.14	24.2	71.8	19.8